Energetics of Assembling an Artificial Heterodimer with an α/β Motif: Cleaved versus Uncleaved *Escherichia coli* Thioredoxin†

Roxana E. Georgescu,‡ Emory H. Braswell,§ Dan Zhu,§ and María Luisa Tasayco*,‡

Biochemistry Division, Chemistry Department, City College of the City University of New York, New York, New York 10031, and National Analytical Ultracentrifugation Facility, Biotechnology Center, University of Connecticut, Storrs, Connecticut 06269

Received March 3, 1999; Revised Manuscript Received July 12, 1999

ABSTRACT: We have studied the folding/binding process between the N- and C-fragments (1−73, 74−108) of oxidized *Escherichia coli* thioredoxin (Trx) to compare the energetics between the cleaved and uncleaved Trx. Sedimentation equilibrium analysis in 0.1 M potassium phosphate, pH 5.7, shows (i) the strong and weak self-association of the N- and C-fragments, respectively, (ii) a heterodimer with a small dissociation constant (K_d) ca. 100 nM, and (iii) monomeric Trx. To avoid self-association, measurements were carried out in 10 mM potassium phosphate, pH 5.7. Far-UV CD spectra of the fragments at variable temperature show an isodichroic point at 208 nm and a non-cooperative cold induced disordering transition without concentration dependence. Deconvolution of these spectra indicates the presence of residual structure. Titration of the N-fragment with an excess of C-fragment indicates a 1:1 stoichiometric complex with an apparent K_d ca. 49 nM. Analysis of this complex by CD and hydrogen exchange/2D-NMR (Tasayco and Chao (1995) *Proteins: Struct., Funct., Genet. 22*, 41−44) spectroscopy indicates the reassembly of the α/β motif of Trx. GnHCl induced unfolding measurements give ΔG^0 values of 9.5 ± 0.2 and 10.0 ± 0.4 kcal/mol at 20 °C for the uncleaved and cleaved Trx, respectively. The far-UV CD melting curve of uncleaved Trx indicates an intriguing non-cooperative upward baseline trend. CCA analysis of these spectra indicates the presence of a native-like folded intermediate. A three-state thermodynamic analysis of the thermal transition curves gives a total ΔH^0 of unfolding of 121 ± 4 kcal/mol at the T_m (88 °C), while the two-state analysis for cleaved Trx gives 122 ± 6 kcal/mol at 88 °C. Analysis of the chemical and thermal unfolding of both proteins indicates a value of ca. 1 M for the apparent effective concentration (C_{eff}) of cleaved Trx.

Protein−protein interactions are central to the regulation of biological phenomena. Analysis of the structural database of proteins indicates that (i) the same hydrophobic folding units are found in monomers and around the protein−protein interface of oligomeric proteins (*1*) and (ii) that Nature finds ways of assembling the same unit using pieces of various shapes and sizes. At first glance, the major difference between folding and folding/binding seems to be the loss of rotational and translational entropy that occurs during binding. Indeed, many groups have attempted to estimate this difference, but there is as yet no consensus about the contributing factors (*2*−*7*).

The evaluation of those contributions is relevant for understanding binding and folding. Careful studies of the reassembly of a hydrophobic folding unit by fragment complementation should help to dissect those contributions. In the last decade, enormous progress has been made in the prediction, based on calorimetric and structural information, of the number of residues that participate in folding/binding events (*8*). However, to understand the determinants for the stability of a hydrophobic folding unit, it is imperative to evaluate in the best way possible the unfolded state. For a long time, studies have focused on how interactions stabilize a native protein (*9*). And it is only recently that studies on the unfolded state of proteins have begun to indicate that this state is more complex than originally suspected (*10*). Heterodimers are particularly suitable to investigating the unfolded state since one can study the folded dimer and the unfolded monomers under the same conditions. This analysis does not rely on extrapolations from chemically and/or thermally induced unfolding processes. However, most techniques do not distinguish among the conformations that constitute the ensemble of the unfolded state and thus provide only an average value. We have chosen oxidized *Escherichia coli* thioredoxin (Trx),[1] a small single α/β-domain monomeric protein with cis P76, as a model system to study the effect of the site of cleavage on the reassembly of complementary fragments. We have shown at atomic detail the reassembly after cleavage of a loop (1−73, 74−108) (*11*)

† This work was supported by the RCMI grant from NIH to CCNY, NSF grant (MCB-9507255) to M.L.T., who is an NSF CAREER Awardee, and NSF grant (BIR 9318373) to the National Analytical Ultracentrifugation Facility.

* To whom correspondence should be addressed.

‡ City College of the City University of New York.

§ University of Connecticut.

[1] Abbreviations: ANS (8-anilino-1-naphthalenesulfonic acid); CCA, convex constraint algorithm; CD, circular dichroism; GnHCl, guanidinium hydrochloride; ISS, the ideal single species model; Trx, oxidized *E. coli* thioredoxin; cleaved Trx, the noncovalent complex between N- and C-fragments of Trx (1−73 and 74−108, respectively); TMSP, (2,2,3,3-tetradeuterio-3-(trimethylsilyl)propionic acid sodium salt).

10.1021/bi990498l CCC: $18.00
Published on Web 09/11/1999

and an α-helix (1−37, 38−108) (*12*). Both sets of fragments are typically disordered under physiological conditions and produce the same hydrophobic folding unit but with a dramatically different interface geometry.

In this article, we have compared the energetics between uncleaved Trx and its cleaved version (1−73/74−108). Far- and near-UV CD, fluorescence, and 1D-NMR spectroscopy were used to perform thermally and chemically induced unfolding measurements. Three types of experiments, including titration measurements, were used to estimate the energetics between cleaved Trx and its isolated fragments. A discussion on the implications of having a range of effective concentration values for cleaved small single domain proteins is presented.

MATERIALS AND METHODS

Purification of Trx and Its Fragments. Expression of Trx and its fragments was performed according to previously reported procedures (*13*) to achieve at least 95% purity. Amino acid and mass spectroscopy analyses confirmed the homogeneity of the purified fragments and were in good agreement with the molecular weight calculated from the primary sequence. The molar extinction coefficients of the N- and C-fragments used to prepare cleaved Trx were: $\epsilon_N^{280} = 1.41 \times 10^4\ M^{-1}\ cm^{-1}$ and $\epsilon_C^{215} = 3.97 \times 10^4\ M^{-1}\ cm^{-1}$, respectively.

Sedimentation Equilibrium. Solutions of proteins in 7.6 M urea, 10 mM potassium phosphate, pH 7.4, were exchanged into 0.1 M potassium phosphate, pH 5.7, using a G-25 column.

(a) Uncleaved Trx and N-Fragment. Approximately 100 μL of each sample concentration (0.083, 0.167, and 0.33 mg/mL for the N-fragment and 0.1 and 0.3 mg/mL for uncleaved Trx) was loaded into three of the six channels of a cell with quartz windows (12 mm path length), producing a solution column height of ca. 2.5 mm. Fluorocarbon oil (M&M FC-43) (15−25 μL) was added to the samples. The solvent channel of each cell was filled with ca. 120−130 μL of buffer. The gradients were measured at 250 and 280 nM. The cells were centrifuged to equilibrium at 25 and 45 krpm for the N-fragment and 38 and 50 krpm for uncleaved Trx in the Beckman XL-A analytical ultracentrifuge at 20 °C. Absorption data were taken radially at 0.001 cm intervals. Scans were made every 3 h. The PC program "MATCH" (developed by D. A. Yphantis) was used to determine the equilibrium point.

(b) C-Fragment. Longer column height and higher speeds were used to detect self-association. To detect the concentration gradient, Beckman XLI analytical ultracentrifuge with interference optics was used. Sapphire windows were used to reduce the effect of strain.

The cells were "aged" (*14*) until steady conditions were obtained. Aliquots (170 μL) of the fragment solution (0.1 or 0.33 mg/mL) were loaded into three separate cells with ca. 30 μL FC-43, producing a solution column of ca. 4.2 mm. The solutions were centrifuged to equilibrium using 48 and 60 krpm at 20 °C. Water−water blanks were taken at the same experimental conditions and were subtracted from the data.

(c) Cleaved Trx. Both absorption (as with N-fragment) and interference optics (as with C-fragment) were simultaneously used to detect the N-fragment and its complex with the C-fragment. Sapphire cells were used to measure at 250 and 280 nm. Longer solution column heights (ca. 6 mm) were used to improve the detection of the free fragments due to the dissociation/unfolding of the complex. The concentrations used were ca. 0.05, 0.1, and 0.2 mg/mL of equimolar mixtures. The solutions were centrifuged to equilibrium at 38 krpm at 20 °C.

Circular Dichroism and Fluorescence. All spectroscopic measurements were performed in 10 mM potassium phosphate, pH 5.7 (KP_i), at 20 °C, unless otherwise mentioned. The protein concentrations are given in terms of monomers unless indicated otherwise. (i) Far-UV CD spectra of isolated fragments and uncleaved and cleaved Trx at different concentrations were obtained with an AVIV-60DS instrument equipped with a thermostatic cell holder and cells of 1 or 2 mm pathlength. The spectra represent the average of five scans at 20 nm/min after subtracting the buffer baselines. Additionally, near-UV CD spectra of cleaved and uncleaved Trx were acquired, averaged, and corrected. (ii) Intrinsic fluorescence emission spectra of Trp28 and Trp31 and ANS emission spectra were recorded on a PTI spectrofluorimeter at 20 °C, using the appropriate slit width settings (1−5 nm band-pass).

Stoichiometry. The stoichiometry of cleaved Trx in KP_i was determined by 1D-NMR titration measurements. Increasing amounts of C-fragment were added to 50 μM N-fragment in KP_i with 90% H_2O/10% D_2O and TMSP. Afterward, 800 scans were acquired on a 500 MHz Varian Unity plus spectrometer following a S2pul sequence with presaturation at 20 °C. The stoichiometry was determined using the plot of the area under the up-field peaks versus the ratio between C- and N-fragments.

Apparent Dissociation/Unfolding Constant. Increasing amounts of C-fragment were added to 0.9 μM N-fragment to reach 0.1−6 μM of C-fragment. The fluorescence of the mixtures was measured after 3 h incubation at 20 °C. Controls of C-fragment were recorded under the same experimental conditions. All the measurements were carried out in low binding tubes. The dissociation/unfolding constant (K_d) of cleaved Trx was calculated by fitting the normalized plot of the measured fluorescence change of N-fragment to the following equation:

$$\Delta F_{meas} = {}^1/_2 \Delta F_{int} \left([N]_0 + [C]_0 + K_d - \sqrt{([N]_0 + [C]_0 + K_d)^2 - 4[N]_0[C]_0}\right) \quad (1)$$

where $[N]_0$ is the total concentration of N-fragment (constant), $[C]_0$ is the concentration of C-fragment, and ΔF_{int} is the difference of intrinsic fluorescence between isolated N-fragment and cleaved Trx.

Chemically Induced Unfolding. GnHCl induced unfolding of cleaved and uncleaved Trx in KP_i was monitored by fluorescence and CD (2.33, 5, 15, and 25 μM). Three fluorescence scans were acquired between 320 and 400 nm at 120 nm/min, averaged, and corrected by subtracting the spectrum of the buffer. Analogous measurements of the change in ellipticity at 222 nm were carried out with an Aviv 60DS at 20 °C. Control for the GnHCl-induced conformational change of N-fragment was also monitored under the same experimental settings.

Thermally Induced Unfolding. Far- and near-UV CD as well as 1D-NMR spectroscopy were used to monitor changes of the fragments and cleaved and uncleaved Trx upon heating.

(a) 1D-NMR spectra were acquired for a 1:1 stoichiometric mixture containing 0.45 mM of each fragment in KP_i/D_2O with TMSP and uncorrected pH. Then, 128 scans were acquired on a 600 MHz Varian Unity plus spectrometer using a S2pul sequence, a spectral width of 9600 Hz, 45 pulse angle, and 45 μs of pw. The total acquisition time was 3 s (giving a total of 57 600 number of points). The relaxation time used was 2 s to permit quantitative integration of the area under the peak. The sample was equilibrated at each temperature for 20−25 min prior to acquisition. The temperature range was 35−78 °C with a step of 2°. Reversibility of thermal denaturation was verified by cooling down to 60 °C and lower temperatures and then comparing the spectra acquired before and after thermal unfolding. The temperature was determined by building a standard calibration curve with ethylene glycol, where the temperature is estimated from the difference between the chemical shifts of the protons for CH_2 and OH (*15*). The proton chemical shifts were calibrated on the TMSP signal. Integration of the relevant peaks from the aromatic and up-field region was performed using as reference the TMSP peak. The relative values of integration were plotted as function of temperature.

(b) The temperature dependence of the CD spectrum for cleaved and uncleaved Trx at different concentrations (5−200 μM) was followed in two ways. First, the ellipticity was monitored at 222 nm while the temperature of the cuvette was either lowered or increased at a rate of 1 °C/min to cover a temperature range (20 to ∼90 °C). The selected rate was sufficient to assure the necessary equilibration time. Second, the entire spectrum (near- or far-UV region) was monitored at various temperatures with a 5−10 °C increment and 10 min equilibration time. The temperature dependence of the fragments was performed within a 10−100 μM concentration range and between −3 to 80 °C. The acquired scans were corrected with the spectra for the buffer.

DATA ANALYSIS

(a) Sedimentation Equilibrium. Data analysis was performed using a nonlinear least squares program Non-Lin (*16*). Global fits were achieved by combining the data sets taken at different loading concentration and speeds and using the appropriate normalization factors. The data fitting was performed using various models, i.e., the ideal single species model (ISS) and self-association models. If the ISS fit is good (low rms and systematic error), the result is the reduced molecular weight (M') of the single species ($M' = M(1 - \bar{\nu}\rho)$), where M is the molecular weight, $\bar{\nu}$ is the specific volume, and ρ is the density of the buffer. If the fit is poor, a z-average M' (M'_z) of all species is produced. The self-association models provide the value of M' for the associating molecule and other constants (i.e., equilibrium constants, second virial coefficient, etc.) as well as the rms error. The equilibrium constant of association is expressed as ln K_a, where K_a is in units of $(L/g)^{n-1}$ and n is the degree of association. The values of $\bar{\nu}$ and ρ are used to convert M' (or M'_z) into M (or M_z). The value of $\bar{\nu}$ was estimated from amino acid composition data (*17*) for the N- and C-fragment and uncleaved Trx (0.743, 0.771, and 0.751 mL/g, respectively).

(b) Chemically Induced Unfolding. Data from GnHCl induced dissociation/unfolding were fitted according to equations for simultaneous dissociation/unfolding processes, which assume a 1:1 stoichiometry for the noncovalent complex (*18*)

$$\mathrm{NC} \overset{K_D}{\rightleftharpoons} \mathrm{N} + \mathrm{C}$$

where $K_D = K_d(D)$, the dissociation/unfolding equilibrium constant at a concentration of denaturant [D], is

$$K_D = \frac{[N][C]}{[NC]} = \frac{P_t f_u^2}{2(1 - f_u)} \quad (2)$$

and f_u is the fraction of unfolded/dissociated complex

$$f_u = \frac{[N] + [C]}{P_t} \quad (3)$$

$P_t = 2[NC] + [N] + [C]$ is the total protein concentration (P_t) expressed in terms of monomer. Algebraic manipulation of the above expressions results in a second-order equation, where the root gives the value of the unfolded fraction as a function of the K_D and P_t:

$$f_u = -\frac{K_D}{P_t} + \sqrt{\left(\frac{K_D}{P_t} - 1\right)^2 - 1} \quad (4)$$

Given that $K_D = K_d(D) = \exp(-\Delta G_D^0/RT)$ and assuming that (*19*) $\Delta G_D^0 = \Delta G^0 + m[D]$, where ΔG^0 is the extrapolated standard free energy of dissociation/unfolding in the absence of denaturant, the dependence of f_u upon the denaturant concentration can be obtained by fitting the data with the nonlinear squares fitter from the Fig.P (Biosoft, UK) or Microcal Origin software packages, according to the equation

$$y_{obs} = f_u(y_u + m_u[D]) + (1 - f_u)(y_f + m_f[D]) \quad (5)$$

where y_{obs} is the observed molar signal, y_u and y_f are, respectively, the molar signals for the unfolded and folded states, and m_u and m_f are the slopes of the corresponding baselines. From the extrapolation to zero denaturant, one can thus obtain an estimate of the $K_d = K_d(0)$ value.

(c) Thermally Induced Unfolding. Assuming that the heat capacity (ΔC_p) is approximately constant over the temperature range (20−80 °C) of the experimental data (*20*), the unfolding traces were fitted to theoretical curves using the same two-state transition approach and the following equation

$$\Delta G_T = \Delta H_T - \frac{T}{T_m}\left(\Delta H_T - RT_m \ln\left(\frac{P_t}{4}\right)\right) + \Delta C_p\left(T - T_m - T\ln\left(\frac{T}{T_m}\right)\right) \quad (6)$$

ΔH_T and ΔG_T are the standard enthalpy and standard free energy of unfolding; the ΔC_p value of uncleaved Trx (1.66 kcal mol^{-1} K^{-1}) (*21*) was used for data fitting of both uncleaved and cleaved Trx. The melting profiles of uncleaved

Trx were additionally analyzed according to a three-state transition mechanism, involving a monomeric intermediate:

$$F \overset{K_1}{\rightleftharpoons} \mathrm{I} \overset{K_2}{\rightleftharpoons} \mathrm{U}$$

The molar fraction of each specie (f_f, f_u, and f_i) can be expressed in terms of the equilibrium constants for the unfolding reaction (K_1 and K_2) as follows:

$$f_u = \frac{K_1 K_2}{1 + K_1 + K_1 K_2} \quad (7)$$

$$f_i = \frac{K_1}{1 + K_1 + K_1 K_2} \quad (8)$$

$$f_f = \frac{1}{1 + K_1 + K_1 K_2} \quad (9)$$

The observed spectroscopic signal at a given temperature was expressed as a linear combination of the molar signal from each species (y_u, y_i, and y_f) according to the following equation:

$$y_{obs} = f_u(y_u^0 + m_2 T) + f_i y_i + f_f(y_f^0 + m_1 T) \quad (10)$$

The contribution of the folded and unfolded were assumed to be linearly dependent on temperature within the experimental range, while y_i was considered temperature independent. Nonlinear least squares fitting of the above equations to the experimental or normalized data using Microcal Origin script provided the following parameters: ΔH_1 and ΔH_2 (standard enthalpy for each transition), ΔC_{p1} and ΔC_{p2} (heat capacity for each transition), T_{m1} and T_{m2} (midpoint temperatures), m_1 and m_2 (slopes for the pre- and post-transition baselines, respectively), and y_f^0 and y_u^0 (molar signals at 0 °C).

RESULTS

Sedimentation Equilibrium. To study the non-self-association of the N- and C-fragments it is first necessary to understand the self-association of each of the isolated fragments. Therefore, sedimentation equilibrium studies were conducted on the isolated fragments, their approximate equimolar mixture, and uncleaved Trx. Potassium phosphate (0.1 M) at pH 5.7 was chosen for two reasons: (i) to avoid charge nonideality problems and (ii) to mimic the conditions of the NMR experiments and molecular sieve chromatography (data not shown) which indicate the presence of monomeric and dimeric species.

(a) N-Fragment. Six sets of data (ca. 695 points) covering a concentration range from 0.01−0.02 mg/mL to ca. 0.5 mg/mL were fitted globally using the Non-Lin program. The ISS fit produced a value of M_z greater than 12 times that of the fragment (8068 Da). The best fit to all the data was that of monomer-trimer-24mer (M_{24} = 193 kDa) with no visible systematic error. The M value for this monomer was 9.1 ± 0.2 kDa (95% confidence limits). The values for ln $K_{a,1-3}$ and ln $K_{a,1-24}$ were 7 ± 6 and 82 ± 39, respectively. These large errors reflect a wide range of ln K_a values (one for each loading concentration and speed) which is common for complex aggregations. This, together with the poor value of M indicate the nonspecificity of the association constants and imply heterogeneity in either K_a or M. It is plausible that some species are noncompetent to either self-associate or dissociate. Less good fits (i.e., monomer-dimer-24mer) produced a better M value for the monomer (8.1 ± 0.8 kDa).

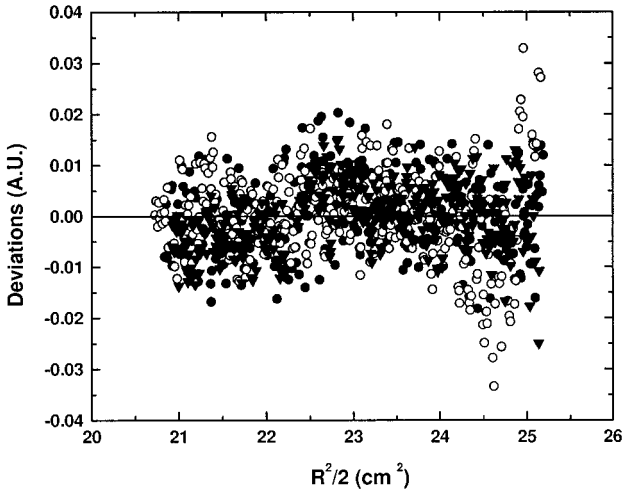

FIGURE 1: Analysis of the sedimentation equilibrium measurements for a 1:1 stoichiometric mixture of N- and C-fragments using absorbance at 280 nm gives this residual plot of deviation from the ISS model as a function of position in the cell. The loading concentrations were: 0.05 mg/mL (filled circles), 0.1 mg/mL (empty circles) and 0.2 mg/mL (filled triangles) in 0.1 M potassium phosphate, pH 5.7.

(b) C-Fragment. Six sets of data (ca. 3617 points) covering a concentration range from ca. 0.05 mg/mL to ca. 4.22 mg/mL were fitted (0.089 fringes rms error), producing a M_z value of 4.57 ± 0.19 kDa (ca. 25% larger than the monomer, i.e., 3630 Da). The best fit was obtained for a monomer-pentamer (0.018 fringes) with no visible systematic error. This fit gave a M value for the monomer of 3.67 ± 0.02 kDa and a value for ln $K_{a,1-6}$ of −3.4 ± 1.2. This study clearly shows that the self-association of C-fragment is weak.

(c) Uncleaved Trx. Six sets of data (ca. 1022 points) covering a concentration range from ca. 0.05 mg/mL to ca. 3 mg/mL yielded a good fit (rms error 0.008 au). This fit produced a M_z value of 11.1 ± 0.3 kDa, indicating a homogeneous M and little or no self-association.

(d) Cleaved Trx. Fitting three sets of absorbance data (1037 data points) globally yielded a value of 10.9 ± 0.3 kDa for M_z (rms error of 0.009 au), while the interference data (2403 points) yielded 11.7 ± 0.3 kDa (rms error of 0.024 fringes) (see Figure 1). These results indicate a 1:1 stoichiometry. Absorption measures the sum of the concentrations of bound and free N-fragment, while interference measures the sum of the concentrations of all fragments. Therefore the linearity of plots of ln C vs $r^2/2$ for both optical systems over the observable concentration (C) range and within the range of radial position of a molecule in the cell (r) indicates that M is constant and that the reaction is almost complete. By subtracting, at each radial position, the concentration obtained by absorption from that obtained by interference optics, one can obtain the sum of the concentrations of the bound and free C-fragment at that position. Because the value of M changes from ca. 3.6 to 11.6 kDa with complex formation for the C-fragment as opposed to the smaller change for the N-fragment (ca. 8.1 to 11.6 kDa), a plot of ln C displays some curvature, for the lowest loading concentration experiment, indicating slight association. The estimated K_d value

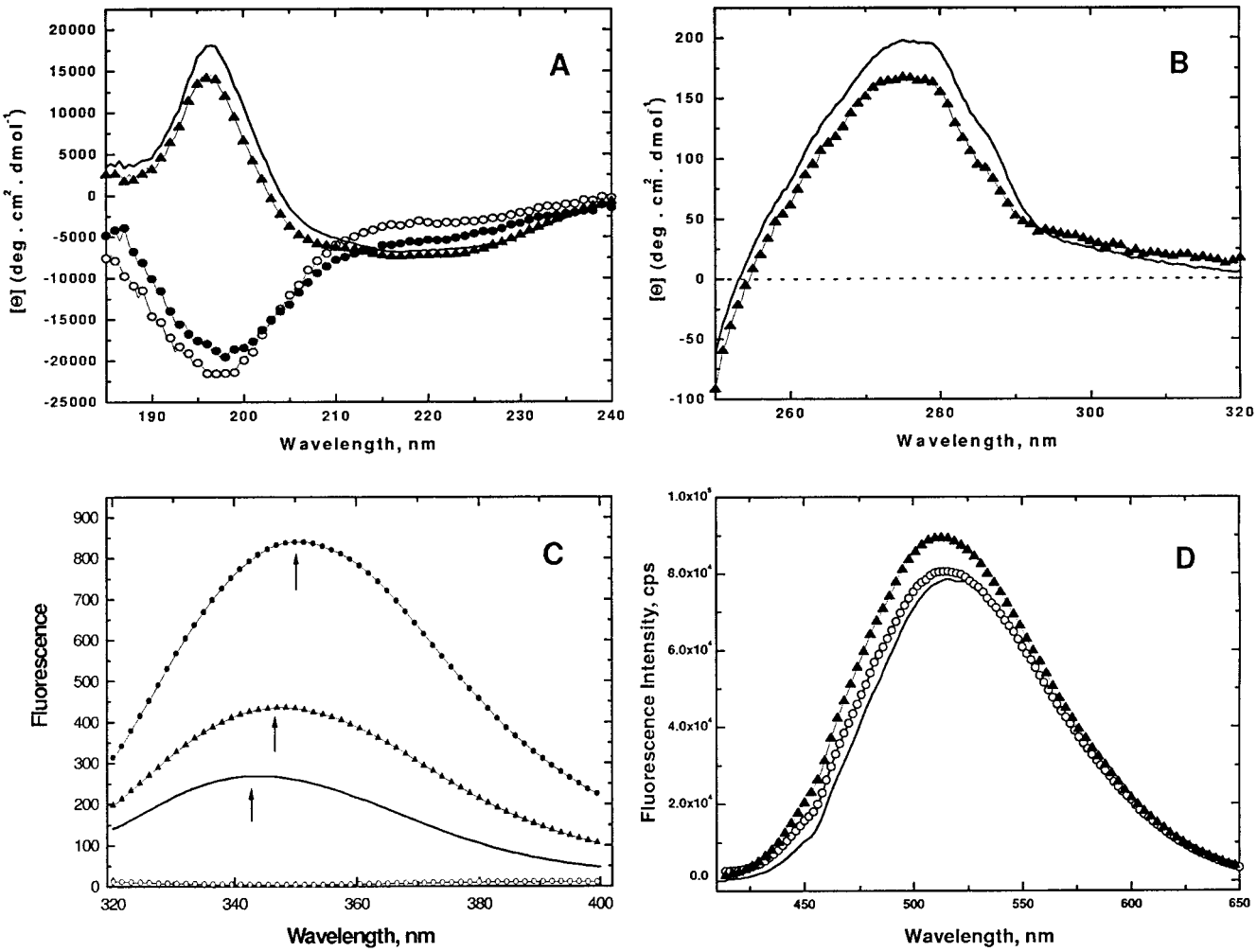

FIGURE 2: The protein concentration was 20 μM in KP_i unless otherwise indicated. All the spectra represent average of five scans corrected by subtracting the spectrum of KP_i. (A) Far-UV CD spectra of the isolated N- and C-fragments (N, filled circle; C, empty circle), cleaved (filled triangle) and uncleaved Trx (line). (B) Near-UV CD spectra of cleaved (filled triangle) and uncleaved Trx (line). (C) Fluorescence emission spectra of 16 μM N-fragment and cleaved and uncleaved Trx. (D) Extrinsic fluorescence emission spectra of a mixture with 12 μM ANS and 2 μM cleaved (filled triangle) or uncleaved Trx (empty circle) in KP_i. The control spectrum of 12 μM ANS in KP_i (line) is given.

is ca. 100 nM. The concentration of free C-fragment is so low that self-association is negligible. Self-association of N-fragment is eliminated by the subtraction.

Clearly the buffer used for sedimentation equilibrium studies produced oligomers of each isolated fragment, but it led us to find lower ionic strength conditions (i.e., KP_i) that favor the monomers. Unfortunately, these new conditions are unsuitable to carry out sedimentation equilibrium measurements due to charge non-ideality problems.

Structural Characterization of Unfolded and Folded States for Cleaved and Uncleaved Trx. These proteins were characterized by far-UV CD at 20 °C in the presence and absence of chemical denaturant (see Figure 2A and Figure 1, Supporting Information). The spectra of the isolated N- and C-fragments indicate the typical features of a disordered fragment at 20 °C and lower temperatures. Indeed, the 1D-NMR spectra of isolated fragments (Yu et al., unpublished results) indicate a narrow dispersion of the amide region and sharp resonances, which are typical of disordered states. However, the large difference between the "sum spectrum" of the N- and C-fragments and that of their equimolar mixture indicates a folding/binding event. The similarity between the latter one and that of uncleaved Trx suggests complete recovery of secondary structure. Molecular sieve chromatography (data not shown) and titration NMR experiments using the up-field resonances of the 1D-NMR spectrum for the equimolar mixture confirmed the 1:1 stoichiometry of the complex (Figure 3A). The intrinsic fluorescence of the N-fragment (Trp28 and Trp31) is quenched by the addition of C-fragment (no Trp), and its λ_{max} is blue-shifted (Figure 2C). Additionally, the ANS emission spectrum is not affected by adding an equimolar mixture of fragments or uncleaved Trx (Figure 2D), suggesting a native-like burial of hydrophobic side chains in the folded state. Previous hydrogen exchange/2D-NMR studies (*11*) of cleaved Trx and recent multidimensional NMR studies (Yu et al., unpublished results) demonstrate the presence of the native super-secondary structure with defined packing of side chains and subtle local differences around the cleavage site.

The minimum at 197 nm of the far-UV CD spectra for both fragments is indicative of disordered structure. However, changes in the ellipticity of the shoulder at 215 nm (Figure 1, Supporting Information) due to 4 M GnHCl suggest the presence of residual structure. Analysis of these spectra using various deconvolution methods (Table 1)—K2D (*22*), Contin (*23*), or MLR (*24*)—indicates that the N-fragment is globally

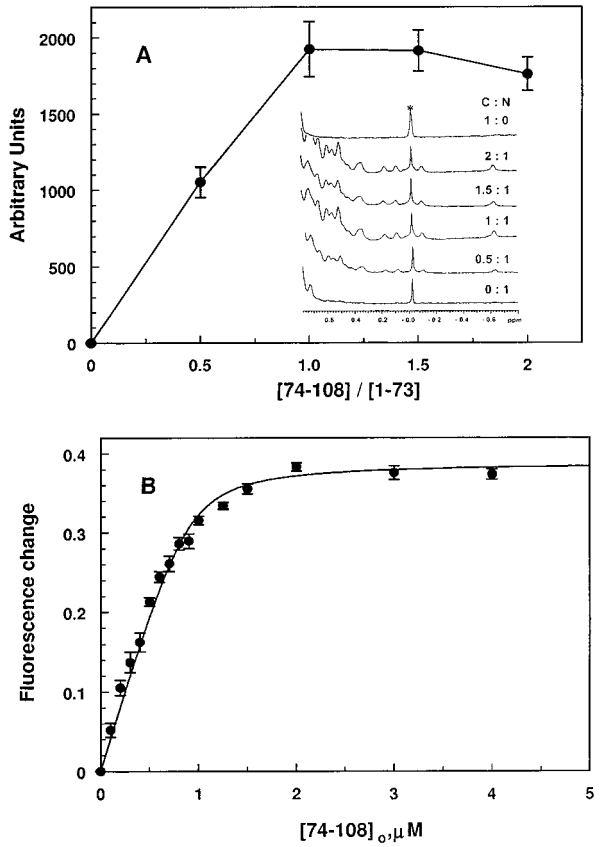

FIGURE 3: (A) Stoichiometry of cleaved TRX monitored by 1D-NMR. The inset shows the up-field region and the apparition of characteristic resonances for the complex, obtained by the titration of 50 μM N-fragment in KP_i in 90% D_2O/10% H_2O, with different amounts of C-fragment. The integration of the peaks was performed using as reference the TMSP. (B) Apparent dissociation constant for cleaved Trx. Equilibrium association of N- and C-fagments (filled circle) was monitored by quenching the fluorescence emission at 350 nm. The reactions were carried out using 0.9 μM N-fragment in KP_i at 20 °C. The data points represent the average of four independent experiments. The solid curves represent the best fits according to eq 1.

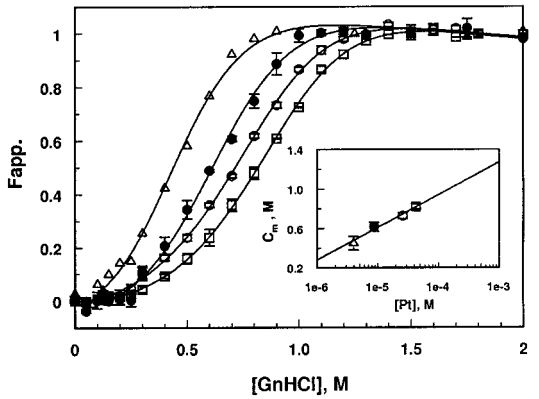

FIGURE 4: Chemical denaturation of cleaved Trx. Concentration dependence of GnHCl-induced unfolding of cleaved Trx at 2.33 μM (empty triangle), 5 μM (filled circle), 15 μM (empty circle) and 25 μM (empty square) in KP_i at 20 °C. The fraction of unfolded cleaved Trx (Fapp) was calculated according to a two-state transition process using the intrinsic fluorescence at 350 nm and ellipticity at 222 nm. The data represent the average of three to five experiments. The inset shows the linear dependence of the estimated C_m with the logarithm of protein concentration.

Table 1: Secondary Structure Analysis of Fragments and Cleaved and Uncleaved Trx

protein	method	% α-helix	% β-sheet	% turns	others
N	K2D	6.0	29	*a*	65.0
	Contin	4.0	14.0	10.0	72.0
	Mlr (Brahms)[b]	2.5	28.7	10.3	58.5
C	K2D	2.0	16.0	*a*	82.0
	Contin	3.0	11.0	1.0	86.0
	Mlr (Brahms)[b]	0.0	15.7	0.0	84.3
NC	K2D	30.0	20.0	*a*	50.0
	Contin	20.0	40.0	7.0	34.0
	Mlr (Fasman)[b]	22.8	23.7	9.2	21.8; 22.5[c]
	Selcon	24.66	21.53	16.86	22.5[c]
Trx	K2D	27.0	25.0	*a*	48.0
	Contin	18.0	37.0	8.0	37.0
	Mlr (Fasman)[b]	31.8	22.9	7.2	16.9; 21.2[c]
	Selcon	28.35	24.8	24.37	21.44
	X-ray data[d]	40.0	28.25	14.0	17.75

[a] Undetermined. [b] Selected Database. [c] Estimate of aromatic and disulfide bond contributions. [d] Based on molecule A of the PDB file 2trx.pdb (*25*).

more structured than the C-fragment at 20 °C with an average content richer in β-type structures, turns, and/or strands (25 ± 5%) than α-helical ones (4 ± 2%). Moreover, the spectra of the isolated fragments seem to depend on the type of denaturing agent, i.e., GnHCl or temperature. Both fragments appear to follow a non-cooperative cold induced disordering transition (Figure 5) and their far-UV CD spectra at −3 °C (Figure 5, inset) do not overlap with that of 4 M GnHCl (data not shown). Analysis of their spectra at 80 °C (Figure 5, inset) using various deconvolution programs (Contin, K2D, MLR) gave 31 ± 5%, 30 ± 4% of β-type structures and 9 ± 3%, 7 ± 2% of α-helix for the N- and C-fragments, respectively. Thus, the degree of residual structure in the isolated fragments increases upon heating.

On the other hand, deconvolution of the spectra of the cleaved Trx shows approximately 24 ± 5% of α-helix, 26 ± 4% of β-strands, and 11 ± 7% of β-turns (Table 1). These results, however, differ from the calculations of α-helical content in uncleaved Trx based on X-ray crystallography (*25*) and NMR spectroscopy (*26*, *27*). The near-UV CD spectra of cleaved and uncleaved Trx show a similar maximum in ellipticity at 280 nm (see Figure 2B). Moreover, the ellipticity due to the aromatic side chains of Trx appears to be stronger than for other proteins (Trp repressor (*28*), apo-Myoglobin (*29*), protein HPr (*30*), apolipoprotein A-2 (*31*)) and might be responsible for differences between the expected content of secondary structure according to X-ray data and the results of our deconvolution (Table 1).

Energetics of Cleaved and Uncleaved Trx. To compare the energetics of cleaved and uncleaved Trx, three methods were used: titration measurements and chemical and thermal induced unfolding.

(a) Apparent Unfolding/Dissociation Constant. The titration of the N-fragment with increasing amounts of C-fragment was monitored by quenching its fluorescence (Figure 3B). Data analysis according to eq 1 gave us a value for the K_d of cleaved Trx in KP_i at 20 °C (49 nM).

(b) Chemically Induced Unfolding. The chemical stability of uncleaved and cleaved Trx was determined using far-UV CD and/or Trp fluorescence as a function of GnHCl concentration. Uncleaved Trx follows a two-state unfolding process in GnHCl, and our experimental results (Table 2) agree with previous reports (*21*, *32*). The GnHCl induced

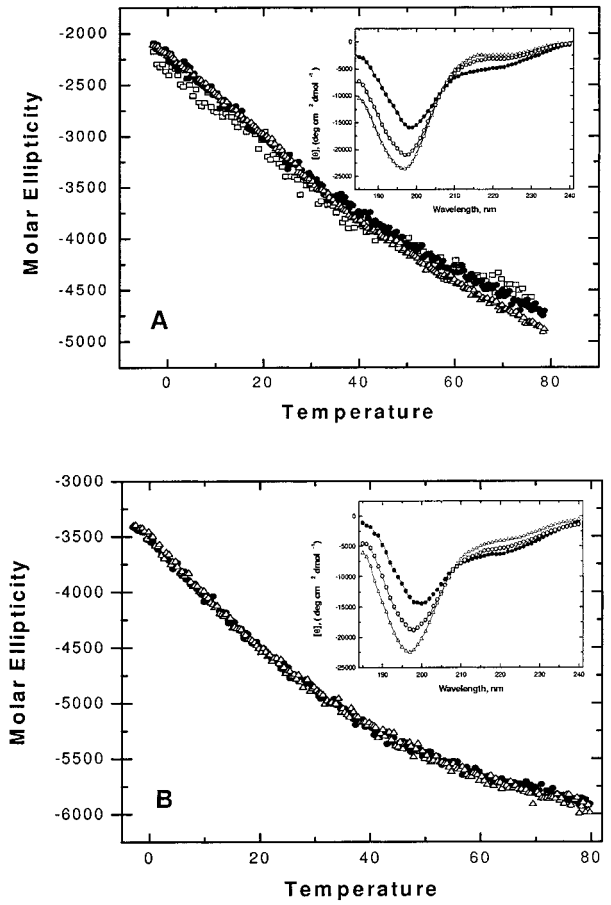

FIGURE 5: Thermal behavior of the isolated fragments. Temperature dependence of the ellipticity at 222 nm for 10 μM (empty square), 50 μM (filled circle), and 100 μM (empty triangle) of C- and N-fragments (A and B, respectively) in KP$_i$ at 20 °C. The insets display the scans of both fragments at −3 °C (empty triangle), 20 °C (empty circle), and 80 °C (filled circle). Spectra represent averages of four scans of 50 μM fragment in KP$_i$.

unfolding/dissociation of cleaved Trx showed the expected concentration dependence (Figure 4) within the concentration range 2.33−25 μM. The overlapping of normalized fluorescence and far-UV CD for cleaved Trx indicates a global two-state dissociation/unfolding process (Table 2). To compare cleaved versus uncleaved Trx, we calculated the effective concentration (C_{eff}) as the concentration of dimer at which both proteins share the same denaturantion midpoint (C_m). Analysis of the concentration dependence of GnHCl induced chemical unfolding/dissociation of cleaved Trx provided a value of 1.0 ± 0.2 M for C_{eff} using values from Table 2 and the following equation:

$$C_{eff} = \exp\left[\frac{1}{RT}\left(\frac{m^{NC}\Delta G^{0,Trx}}{m^{Trx}} - \Delta G^{0,NC}\right)\right] \qquad (11)$$

(c) Thermally Induced Dissociation/Unfolding. The temperature effect on the isolated fragments, Trx, and cleaved Trx was monitored by the change in ellipticity in the far-UV CD (222 nm) and the near-UV CD (280 nm).

The isolated fragments show a gradual non-cooperative thermal transition with enhancement of the content of secondary structure upon temperature increase (Figure 5A,B). This is a concentration independent and completely reversible transition within the concentration range 10−100 μM.

Table 2: Chemical Unfolding of Cleaved and Uncleaved Trx

protein	C_m (M)	ΔG^0 (kcal/mol)	m (kcal/mol M)
Trx	2.61 ± 0.12	9.5 ± 0.2	3.7 ± 0.4
NC		10.0 ± 0.4	3.9 ± 0.3[a]
NC		9.8 ± 0.2[b]	

[a] These values were calculated according to $C_m = (RT \ln P_t + \Delta G^0)/m$ for 2.33, 5, 15, and 25 μM of cleaved Trx. [b] ΔG^0 estimated from titration measurements.

Interestingly, the far-UV CD spectra of both fragments show a clear isodichroic point at 208 nm (Figure 5, inset).

Uncleaved Trx was thermally unfolded at different concentrations (20−160 μM) using far- and near-UV CD at a selected wavelength or in the scan mode. The reversibility of the thermal transition was higher than 95%, and the T_m was essentially independent of the heating rates (0.5 and 1 °C/min). Interestingly, the folded baselines of the two normalized melting profiles do not overlap but the T_m remains the same (Figure 6B). Analysis of the normalized melting curves at different concentrations using a two-state transition gives thermodynamic parameters (Table 3) with no obvious concentration dependence. The values of the ΔH_T at the T_m (ΔH_{Tm}) are in agreement with each other despite the unsatisfactory fitting of the folded baseline for the near-UV CD melting curve, which produces the highest value (126 ± 4 kcal/mol). This two-state transition analysis is in agreement with the CCA (convex constraint algorithm) analysis (*33*) of the far-UV CD spectra for the cooperative part of the thermal transition (80−95 °C), which shows an isodichroic point (Figure 6C, inset). The CCA analysis of the entire family of near-UV CD spectra at various temperatures (Figure 6A) only requires the participation of two pure components, which indicates that the pressumed native-like folded intermediate at 80 °C has essentially the same native tertiary packing. Analysis of the same thermal transition curves (far- and near-UV CD) according to a three-state transition and using a fixed ΔC_{p2} at 1.6 kcal mol^{-1} K^{-1} gives the following thermodynamic parameters: T_{m1} (33.4 ± 6.5 °C), ΔH_1 (13.9 ± 3.4 kcal/mol), ΔC_{p1} (100 cal mol^{-1} K^{-1}), T_{m2} (87.7 ± 1.5 °C), and ΔH_2 (107.2 ± 1.2 kcal/mol). Thus, the value of the standard enthalpy of the cooperative transition at the T_m remains within error essentially the same regardless of the type of analysis.

The thermal dissociation/unfolding of cleaved Trx is reversible. Modification of the scan rate from 0.25 °C/min to 4 °C/min (data not shown) indicated that a rate of 1 °C/min is sufficient to achieve equilibrium since it does not affect significantly the T_m. Analysis of the 1D-NMR spectra of cleaved Trx taken at different temperatures (Figure 7A) shows a subtle variation in the chemical shift of the up-field and aromatic resonances and a distinctive decrease of the area under the resonances with increasing temperature. All the melting curves share the same T_m (data not shown), which suggest a global event. Moreover, the absence of temperature dependence of both chemical shifts and width peaks suggests an exchange between the folded and unfolded states that is slow compared to the NMR time scale ($<10^{-1}$/s).

The family of melting curves for cleaved Trx shows the expected concentration dependence (Figure 7B,D), and the normalized melting profiles (far- and near-UV CD) overlap within experimental error (Figure 7C). Moreover, the CCA

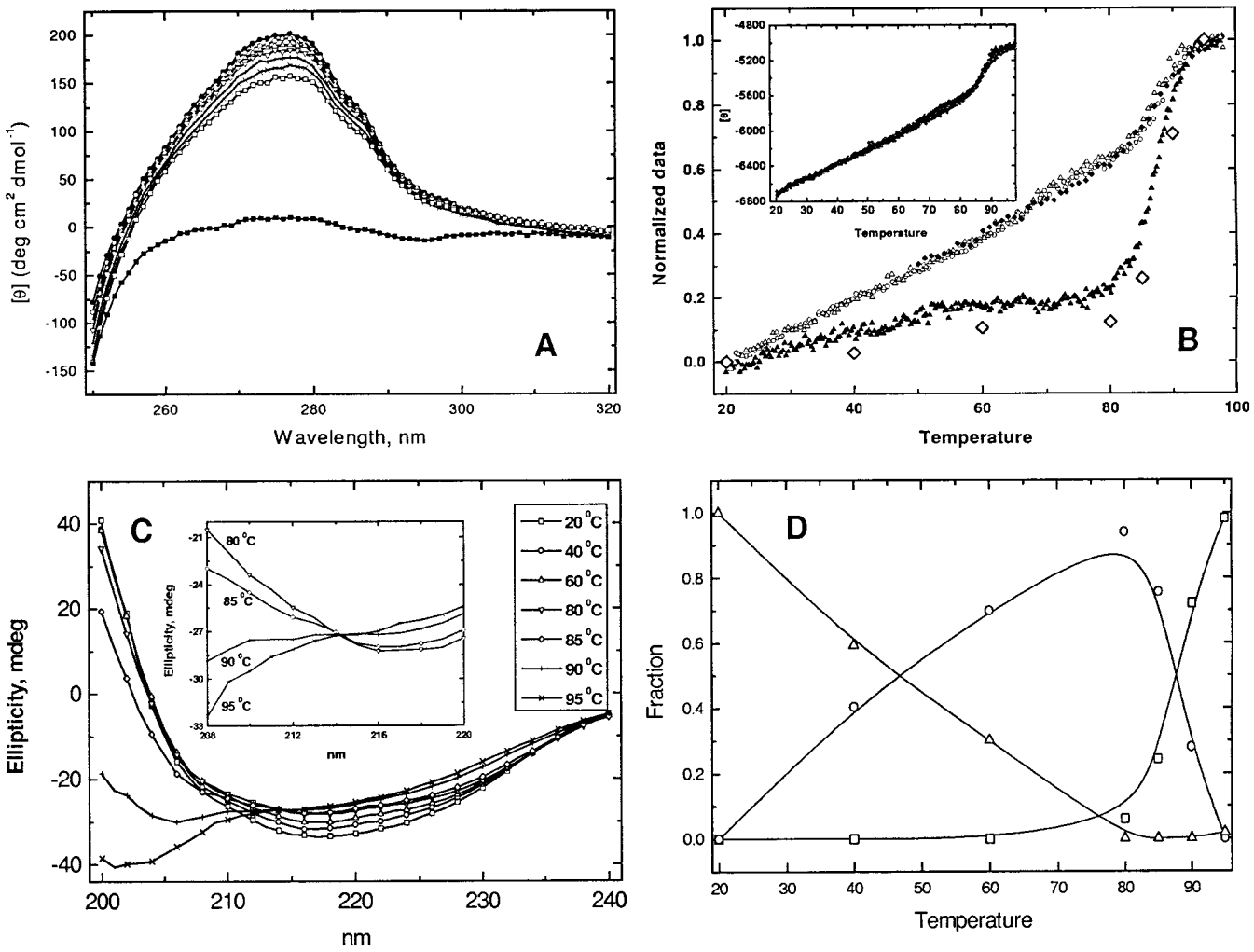

FIGURE 6: Thermal unfolding of uncleaved Trx. (A) Near-UV CD spectra of 80 μM Trx in KP_i at different temperatures (increments of 10 °C) from 20 °C (filled circle) to 90 °C (filled square). (B) Overlay of normalized melting profiles of different protein concentrations in KP_i, (40 μM, filled circle; 80 μM, empty triangle; and 160 μM, empty circle) at 222 nm, 80 μM (empty diamond) at 205 nm, and 80 μM (filled triangle) at 280 nm. Inset: temperature dependence of the molar ellipticity at 222 nm. (C) Far-UV CD spectra of 0.9 mg/mL Trx in KP_i at various temperatures between 20 and 95 °C. The Inset shows a single isodichroic point for the spectra taken within the global unfolding region. (D) The temperature dependent fraction of folded (empty triangle), native-like folded (empty circle), and unfolded (empty squares) states based on the CCA analysis of the family of spectra from panel C.

Table 3: Thermal Unfolding of Cleaved and Uncleaved Trx

protein	conc. (μM)	T_m (°C)	ΔH_{Tm} (kcal/mol)	ΔS_{Tm} (cal mol^{-1} K^{-1})	C_{eff} (M)
Trx	15[a]	88.1 ± 0.1	121.2 ± 4.8	335.6 ± 5.1	
	40[a]	88.7 ± 0.5	116.7 ± 4.2	322.5 ± 7.5	
	80[a]	88.3 ± 0.5	104.5 ± 3.2	289.1 ± 6.8	
	160[a]	87.0 ± 0.4	110.2 ± 3.1	305.9 ± 7.0	
	80[b]	87.9 ± 0.2	125.9 ± 4.4	320.4 ± 6.4	
		88.0 ± 0.6[c]	113.2 ± 6.3[c]	313.3 ± 16.8[c]	
NC	12.5[a]	62.1 ± 0.2	82.9 ± 2.9	223 ± 4	0.5
	20[a]	63.5 ± 0.2	82.1 ± 1.5	223 ± 3	0.7
	40[a]	65.2 ± 0.1	87.9 ± 0.5	240 ± 1	0.8
	80[a]	66.4 ± 0.1	78.5 ± 0.9	214 ± 3	0.7
	160[a]	67.3 ± 0.2	84.1 ± 2.5	230 ± 7	0.8
	450[a]	69.2 ± 0.5	83.5 ± 6.1	229 ± 17	0.9
	80[b]	66.5 ± 0.1	86.8 ± 1.1	235 ± 3	
					0.7 ± 0.2[c]
					0.8 ± 0.4[d]

[a] Analysis of far-UV CD measurements according to a two-state transition and a fixed unfolded baseline. [b] Analysis of near-UV CD measurements according to a two-state transition and a fixed unfolded baseline. [c] Average value of individual measurements at a given concentration. [d] Estimated value of C_{eff} according to the concentration dependence of $1/T_m$.

analysis of the far- and near-UV CD spectra at different temperatures shows that only two components are required to explain the thermal behavior of cleaved Trx. Analysis according to a two-state transition of the thermal dissociation/unfolding curves for cleaved Trx (20 μM and 0.45 mM) gives ΔH_{Tm} and ΔS_{Tm} (Table 3). The extrapolated values of ΔH_T

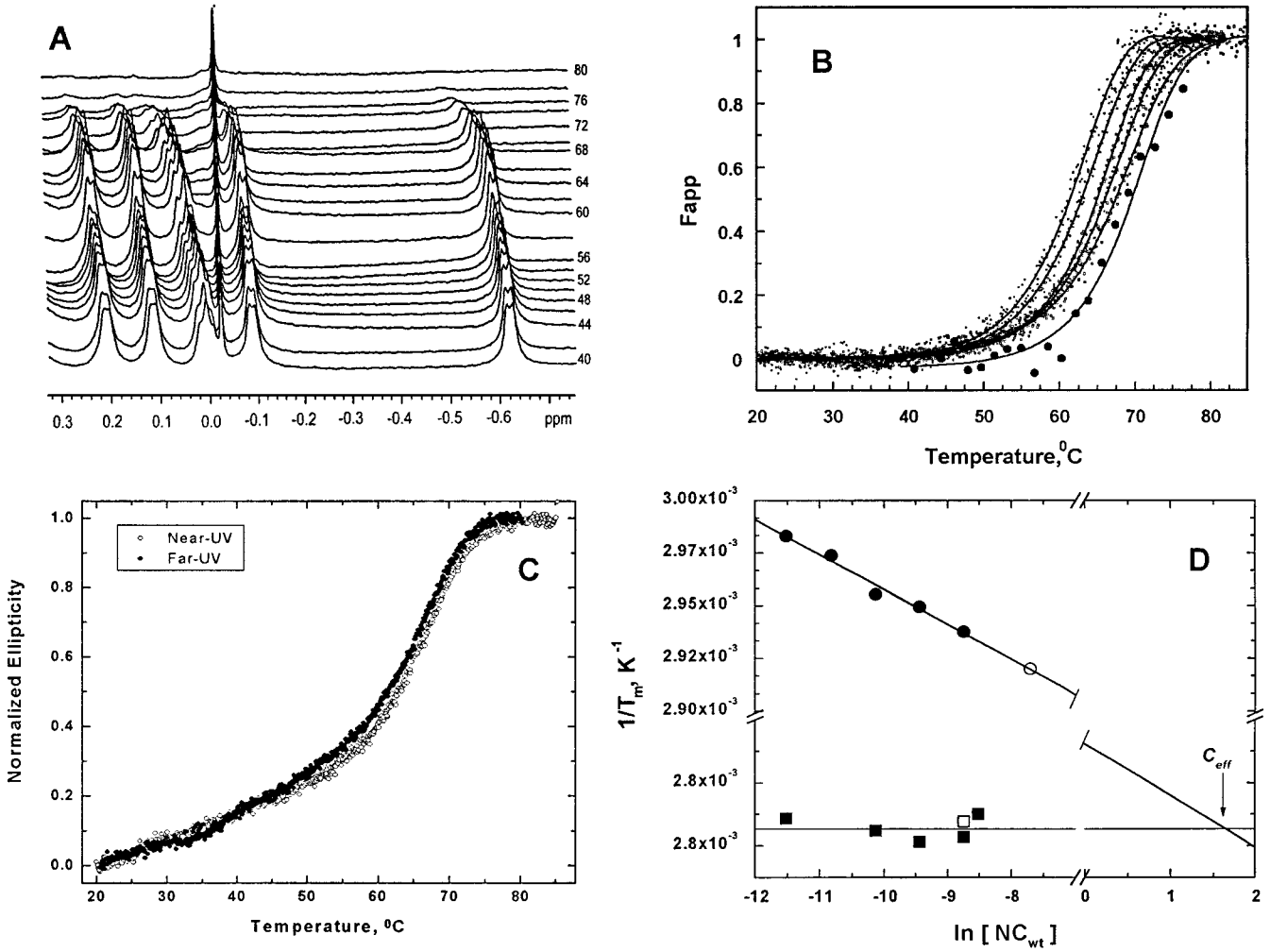

FIGURE 7: Thermal unfolding of cleaved Trx. (A) Stack plot of 1D-NMR spectra for 0.45 mM cleaved Trx in KP_i at various temperatures and a 2 °C interval. Chemical shifts (in ppm) of up-field peaks protons in the folded state at 40 °C are as follows: Val16 H_γ (−0.618), Val16 H_γ (−0.082), Ile72 H_δ (0.016), Leu103 H_δ (0.125), and Val25 H_γ (0.219). (B) Temperature dependence of the unfolded fraction for cleaved Trx according to the ellipticity at 222 nm (20 to 160 μM); the filled circles show the area under the peak of V16 H_γ (0.45 mM). (C) Overlay of normalized melting curves of 2 mg/mL cleaved Trx at 222 and 280 nm. Inset: temperature dependence of the molar ellipticity at 222 nm (80 μM). (D) Concentration dependence of C_m for cleaved (far-UV CD: filled circle; 1D-NMR: empty circle) and uncleaved Trx (far-UV CD: filled square; near-UV CD: empty square).

for the cleaved Trx, at the T_m of the uncleaved, are 122 ± 6 (far-UV CD) and 122 ± 1 kcal/mol (near-UV CD). Likewise, those ones at 65 °C are 82 ± 5 kcal/mol (far-UV CD) and 83 ± 1 kcal/mol (near-UV CD). The value of C_{eff} derived from the plot of the reciprocal of T_m versus the log of protein concentration (0.8 ± 0.4 M; see Figure 7D), is similar to the averaged value obtained from the individual melting curves (0.7 ± 0.2 M, see Table 3).

DISCUSSION

Conformations of Folded and Unfolded States. Despite the obvious lack of structure in the isolated fragments based on far-UV CD and NMR spectroscopy (*12*), many lines of evidence suggest conformational differences between them (i) deconvolution of the far-UV CD spectra indicates an overall greater content of repetitive conformations in the N- than the C-fragment (Table 1). (ii) The N-fragment has three apparently unconstrained Pro and one Pro34 constrained in the trans position by a short range disulfide bond (Cys32−Cys35) while the C-fragment has predominantly a trans Pro76 isomer (Yu et al., unpublished results). (iii) The kinetic model for the association/folding of the complementary fragments indicates that ca. 50% of the N-fragment is slowly exchanging with the competent one (*13*). (iv) Other protein fragments that share the first 37 residues of the N-fragment or the 35 residues of the C-fragment show a far-UV CD spectra (*34*), which is sequence but not length dependent. Together these observations indicate conformational differences between the isolated disordered fragments. Further studies should reveal which residues other than Pro dictate these differences.

Analysis of the far-UV CD spectra of cleaved and uncleaved Trx, and their isolated fragments under the same strong unfolding conditions (chemical and thermal denaturation) (Figures 1 and 2, Supporting Information) further support that each isolated disordered fragment has a distinct conformational preference and that the unfolded states of cleaved and uncleaved Trx show subtle differences between them.

The temperature dependence of the ellipticity at 222 nm for the fragments shows a reversible non-cooperative cold induced disordering transition within this temperature range. This behavior is not due to self-association, since no concentration dependence is observed between 10 and 100

μM in KP_i. However, the N- and C-fragments self-associate strongly and weakly, respectively, in 0.1 M potassium phosphate at pH 5.7, as shown by the sedimentation equilibrium studies. The increase of negative ellipticity at higher temperatures without concentration dependence suggests the presence of certain backbone conformation(s) with marginal stability, which cannot be precisely assessed. This behavior is not unexpected in fragments that have hydrophobic stretches in their sequence, which are difficult to stabilize through native long range interactions. It is plausible that the entire polypeptide chain, under certain unfolding conditions, might also show this behavior. In fact, the temperature dependent stability of the burst phase during the refolding of GuHCl-denatured Trx shows an analogous cold induced transition associated to the hydrophobic effect (*35*). Interestingly, the family of far-UV CD spectra of both fragments at various temperatures (Figure 5A,B, inset) show the appearance of a single isodichroic point at 208 nm, which provides further support for a temperature dependent conformational transition in the disordered state. The features of this thermal transition are complex. On one hand, the single isodichroic point reflects apparently two interconverting populations but the non-cooperativity suggests a stepwise transition. Perhaps each of these populations involve two kinds of species with different number of repetitive units but with the same CD spectrum per unit. A similar behavior has been reported for the so-called PII conformation, a left-handed helix with three residues per turn in peptides, proteins (*36*), and protein/peptide interfaces (*37*).

The similarity between the folded states of both cleaved and uncleaved Trx was observed by NMR (*11*), fluorescence, far- or near-UV CD spectroscopy (Figure 2), and molecular sieve chromatography (*38*). The elution volume of cleaved Trx is smaller than the one for uncleaved Trx, indicating a less compact state for the first one. The ANS fluorescence (Figure 2D), near-UV CD (Figure 2B), and up-field NMR resonances (Figure 3) of the folded state indicate defined packing of the aliphatic side chains against the eight aromatic side chains that are distributed throughout the entire sequence. Despite the similar spectra, subtle changes in the chemical shifts of the upfield NMR resonances between the cleaved and uncleaved Trx (*11*) and the negligible activity of the latter one (*12*) suggest conformational changes in the active site protrusion and packing of aromatic side chains.

Our results show that the unfolded states of the cleaved and uncleaved Trx, as well as their folded states, show subtle differences between them. Thus, it will be important to establish to which degree are these differences affecting the energetics of these proteins.

Energetics. Both proteins undergo a global transition regardless of cleavage (Table 2). These proteins have similar extrapolated ΔG^0 and C_m values at ca. 1 M protein concentration. The extrapolated ΔG^0 value for cleaved Trx from chemical unfolding experiments agrees with the results from titration measurements (Table 2). However, the equilibrium measurements reflect the mixture of cis and trans Pro76 isomers in the folded and unfolded states. The K_d values for the cis and trans isomers derived from kinetic measurements (*13*) are 13.6 nM and 2.5 μM, respectively. Thus, indicating that the K_d value derived from equilibrium measurements (49 nM) is an apparent value that reflects a mixture of 98% cis and 2% trans isomers.

Despite the fact that the temperature dependence of the ellipticity for uncleaved Trx at 222 or 280 nm can be approximated by a two-state process, the folded baseline obtained from far-UV CD measurements shows a non-cooperative upward transition which accounts for ~60% of a rather small total ellipticity change (1800 deg cm^2 $dmol^{-1}$) at 222 nm (Figure 6B inset and 6C). The small magnitude of the total change is due to the counteracting effect of the aromatics (*35*). A CCA analysis of the family of far-UV CD spectra taken within a temperature range from 20 to 95 °C indicates that the spectra can be expressed as a combination of three pure components (Figure 6C,D), corresponding to the folded state at 20 °C, the unfolded state at 95 °C, and a native-like folded state at ca. 80 °C. On the other hand, a similar analysis of the family of near-UV CD spectra requires the participation of two species. The presence of a folded baseline with an unexpected upward trend might be explained by a local non-cooperative conformational change within the protrusion of uncleaved Trx. This protrusion contains cis P76, half of the total number of aromatic residues, and an interconnecting distorted helix (60−69). At first glance, one might consider that the trend of the folded baseline reflects the cis/trans isomerization of the partially exposed cis Pro76. However, kinetic refolding studies of the cleaved (*13*) and uncleaved Trx and their P76A variants (*39*; and Georgescu et al., unpublished results) strongly suggest that this isomerization enhances the negative ellipticity at 222 nm and thus is in disagreement with the experimental results. Another possibility might be the "melting" of the distorted helix which shows weak interactions with aromatic side chains in the native 3D-structure. The above mentioned upward baseline trend is significantly lower than the one expected for a regular helical peptide (125 units/°C) (*40*). However, it might still be consistent with a distorted helix. It is plausible that this melting does not produce a discrete native-like folded intermediate but an ensemble of structures with different unfolded portions of this helix. This ensemble might be in fast exchange within itself and with the native structure, and thus awaits further NMR characterization of uncleaved Trx at increasing temperatures.

The overlapping of thermally unfolding curves of cleaved Trx based on far- and near-UV CD measurements (Figure 7B,C) suggests that its unfolding/dissociation occurs in a single cooperative transition. These folded baselines have a weaker upward trend than the one of Trx. This behavior is consistent with an increase in the flexibility of the protrusion due to the cleavage at R73. Analysis of all thermally unfolding curves for uncleaved and cleaved Trx according to a two-state transition gives a value of 113 ± 6 kcal/mol and an extrapolated value of 122 ± 6 kcal/mol, respectively, for the ΔH_T at ca. 88 °C. If we compare the two proteins at a temperature within the range of the experimental T_m's (i.e., 65 °C), the value of the ΔH_T for uncleaved Trx (ca. 78 kcal/mol) is still lower than the one for cleaved Trx (83 kcal/mol). This tendency is unexpected, considering that the folded states are similar and that cleaved Trx might have weaker interactions. One way to explain it is the fact that the ΔH_T depends on the value of ΔC_p that was used to fit the melting curves. For instance, the calculated ΔC_p value for Trx, based on empirical equations and calorimetric measurements (*20*, *41*), ranges between 1.3 and 1.9 kcal mol^{-1} K^{-1}, while the reported experimental values are: 1.66

kcal mol^{-1} K^{-1} (*21*) and 1.88−2.89 kcal mol^{-1} K^{-1} (*42*). Analysis of the melting curves was then performed with the same ΔC_p of 1.66 kcal mol^{-1} K^{-1}. However, the validity of these assumptions need to be tested by calorimetric measurements. Another explanation might be the presence of oligomers and their effect on the ΔC_p and on the estimated ΔH_T. This possibility can be eliminated for concentrations up to 50 μM of cleaved Trx based on sedimentation analysis. The third possibility might be that the enthalpy change associated with the upward folded baseline trend accounts for the difference between the enthalpies of global unfolding for uncleaved and cleaved Trx. Indeed, the treatment of the melting curves for the uncleaved Trx according to a three-state transition increases the total ΔH_T to ca. 121 kcal/mol, which is close to the averaged value for the cleaved protein (122 kcal/mol) at 88 °C. This behavior might reflect the presence of a strain in uncleaved Trx that drives a local non-cooperative unfolding, but is relieved by cleavage at R73.

Effective Concentration. If the conformations of the unfolded state of both the uncleaved and cleaved proteins are equivalent and their folded states are also equivalent, then most likely the standard enthalpies of unfolding (for uncleaved Trx) and unfolding/dissociation (for cleaved Trx) are the same. In this case, the C_{eff} can be expressed just in terms of the differences in the standard entropies at the C_{m} (or T_{m}). In most cases, the C_{eff} value is not determined experimentally but extrapolated from the concentration dependence of the thermodynamic parameters. Assuming the total ΔH_T or ΔH^0 is similar for uncleaved and cleaved Trx, the extrapolated C_{eff} value lies between 0.7 and 1.0 M.

A review of small single domain monomers or dimers with unfolded and folded states that are not substantially altered after cleavage or linkage reveals a rather wide range of C_{eff} values: cleaved immunoglobulin G-binding domain B1 of streptococcal protein G (1−40/41−56) shows a C_{eff} of 6 M (*43*); cleaved CI-2 range between 20−55 mM for the complex 1−40/41−64 (*44*−*47*); cleaved Trx has a C_{eff} between 0.7 and 1.2 M for 1−73/74−108; cleaved Barnase ranges from 1.4−3.8 M for 1−36/37−110 complex (*48*) or 7.3−11 M for 5−22/23−110 (*49*, *50*). Moreover, the estimated C_{eff} value for homodimeric ArcR (53 residues per subunit) is 2.7 mM (*51*) and that for homodimeric ROP (63 residues per subunit) is 50 μM (*52*).

The loss of translational entropy during the binding and folding of two disordered polypeptide chains is not sufficient to account for the wide range of apparent C_{eff} values for small single domain dimers. One contributing factor might be that the region of the uncleaved protein corresponding to the interface in the cleaved one does not maintain the same number and quality of noncovalent interactions. This seems to indicate that the ΔH^0's are not the same. For instance, cleaved Trx has fewer NOE connectivities at the interface (Yu et al., unpublished results) than Trx. Other factors might be differences between the unfolded states which are difficult to establish at atomic detail. And yet another might be the topology of the folded state and/or the geometry of the interface in the cleaved protein.

CONCLUSION

Our spectroscopic studies demonstrate that the N- and C-fragments bind and fold into a noncovalent complex (artificial heterodimer or cleaved Trx) with the same features as the uncleaved Trx. The isolated fragments appear to have residual structure and to behave as two exchangeable populations. These fragments undergo a non-cooperative cold induced disordering transition. Interestingly, the thermal unfolding of uncleaved Trx shows an unexpected non-cooperative event in the folded state besides the global unfolding and thus it can be fitted to a three-state transition model. Cleaved Trx, on the other hand, undergoes a two-state thermal transition. Uncleaved Trx seems to have a lower ΔH^0 of global unfolding than cleaved Trx. An explanation might be that the cleavage releases some strain that forces a local non-cooperative unfolding in uncleaved Trx. Finally, our results, together with other reports on the native-like reassembly of complementary fragments from small single domain proteins without prosthetic groups, indicate that the loss of translational entropy at the C_{m} (or T_{m}) does not account for the wide range of apparent C_{eff} values.

ACKNOWLEDGMENT

We thank Maurice Eftink and Wayne Bolen for their helpful suggestions. We also thank Norma Greenfield, Mario Amzel, and Themis Lazaridis for their stimulating comments and Jian-Hua Li for his technical assistance. The use of the NMR facility from Hunter and Staten Island College is gratefully acknowledged.

SUPPORTING INFORMATION AVAILABLE

Results from far-UV CD and fluorescence measurements, regarding the residual structure of the individual fragments (Figure 1) and comparison between the thermal and chemical denaturation state of cleaved versus uncleaved Trx (Figure 2). This information is available free of charge via the Internet at http://pubs.acs.org.

REFERENCES

1. Tsai, C. J., and Nussinov, R. (1997) *Protein Sci. 6*, 1426−1437.
2. Steinberg, I. Z., and Scheraga, H. A. (1963) *J. Biol. Chem. 238*, 172−181.
3. Murphy, K. P., Xie, D., Thompson, K. S., Amzel, L. M., and Freire, E. (1994) *Proteins: Struct., Funct., Genet. 18*, 63−67.
4. Tidor, B., and Karplus, M. (1994) *J. Mol. Biol. 238*, 405−414.
5. Brady, G. P., and Sharp, K. A. (1997) *Curr. Opin. Struct. Biol. 7*, 215−221.
6. Tamura, T., and Privalov, P. L. (1997) *J. Mol. Biol. 273*, 1048−1060.
7. Amzel, L. M. (1997) *Proteins 28* (2), 144−149.
8. Spolar, R. S., and Record, M. T., Jr. (1994) *Science 263*, 777−784.
9. Privalov, P. L., and Gill, S. J. (1988) *Adv. Protein Chem. 39*, 191−234.
10. Dill, K. A., and Shortle, D. (1991) *Annu. Rev. Biochem. 60*, 795−825.
11. Tasayco, M. L., and Chao, K. (1995) *Proteins: Struct., Funct., Genet. 22*, 41−44.
12. Yang, X.-M., Yu, W.-F., Li, J.-H., Fuchs, J., Rizo, J., and Tasayco, M. L. (1998) *J. Am. Chem. Soc. 120* (32), 7985−7986.
13. Chaffotte, F. A., Li, J.-H., Georgescu, R. E., Goldberg, M. E., and Tasayco, M. L. (1997) *Biochemistry 36*, 16040−16048.
14. Ansevin, A. T., Roark, D. E., Yphantis, D. A. (1970) *Anal. Biochem. 34*, 237−261.
15. Van Geet, A. L. (1968) *Anal. Chem. 40*, 2227−2229.

16. Johnson, M. L., Correia, J. J., Halvorson, H. R., and Yphantis, D. A. (1981) *Biophys. J. 36*, 575−588.
17. Cohn, E. J., and Edsall, Eds. (1943) *Proteins, Aminoacids and Peptides*, pp 370−381, Reinhold Publishing Corp., New York.
18. Marky, L. A., and Breslauer, K. J. (1987) *Biopolymers 26*, 1601−1620.
19. Pace, C. N. (1986) *Methods Enzymol. 131*, 266−280.
20. Privalov, P. L. (1979) *Adv. Protein Chem. 33*, 167−241.
21. Santoro, M. M., and Bolen, D. W. (1992) *Biochemistry 31*, 4901−4907.
22. Andrade, M. A., Chacón, P., Merelo, J. J., and Móran F. (1993) *Protein Eng. 6*, 383−390.
23. Provencher, S. W., Glöckner, J. (1981) *Biochemistry 20*, 33−37.
24. Brahms, S., and Brahms, J. (1980) *J. Mol. Biol. 138*, 149−178.
25. Katti, S., LeMaster, D. A., and Eklund, H. (1990) *J. Mol. Biol. 212*, 167−184.
26. Dyson, H. J., Holmgren, A., Wright, P. E. (1989) *Biochemistry 28*, 7074−7087.
27. Jeng, M.-F., Campbell, A. P., Begley, T., Holmgren, A., Case, D. A., Wright, P. E., and Dyson, H. J. (1994) *Structure 2*, 853−868.
28. Gloss, L., and Matthews, C. R. (1997) *Biochemistry 36*, 5612−5623.
29. Griko, Y. V., and Privalov, P. L. (1994) *J. Mol. Biol. 235*, 1318−1325.
30. Van Nuland, N. A. J., Meijberg, W., Warner, J., Forge, V., Scheek, R. M., Robillard, G. T., and Dobson, C. M. (1998) *Biochemistry 37*, 622−637.
31. Gursky, O., and Atkinson, D. (1996) *Protein Sci. 5*, 1874−1882.
32. Langsetmo, K., Fuchs, J., and Woodward, C. (1989) *Biochemistry 28*, 3211−3220.
33. Perczel, A., Hollósi, M., Tusnady, G., Fasman, G. D. (1991) *Protein Eng. 4*, 669−679.
34. Yang, X., Georgescu, R. E., Yu, W., Li, J.-H., Haierhan, and Tasayco, M. L. (1999) *Pacific Symposium on Biocomputing*, pp 590-600, World Scientific.
35. Georgescu, R. E., Li, J.-H., Goldberg, M. E., Tasayco, M. L., and Chaffotte A. F. (1998) *Biochemistry 37*, 10286−10297.
36. Sreerama, N., and Woody, R. W. (1994) *Biochemistry 33*, 10022−10025.
37. Siligardi, G., and Drake, A. F. (1995) *Biopolymers (Pept. Sci.) 37*, 281−292.
38. Sevieux, N., and Li, J.-H. (1997) *J. Student Res. CCNY 1*, 25−28.
39. Kelley, R. F., Richards, F. M. (1987) *Biochemistry 26*, 6765−6774.
40. Rohl, C. A., and Baldwin, R. L. (1998) *Methods Enzymol. 295*, 1−26.
41. Becktel, W. J., and Schellman, J. A. (1987) *Biopolymers 26*, 1859−1877.
42. Ladbury, J. E., Wynn, R., Hellinga, H. W., and Sturtevant (1993) *Biochemistry 32*, 7526−7530.
43. Honda, S., Kobayashi, N., Hunekata, E., and Uedaira, H. (1999) *Biochemistry 38*, 1203−1213.
44. Jackson, S. E., el Masry, N., and Fersht, A. R. (1993) *Biochemistry 32*, 11270−11278.
45. de Prat Gay, G., Ruiz-Sanz, J., and Fersht, A. R. (1994) *Biochemistry 33*, 7964−7970.
46. Ruiz-Sanz, J., de Prat Gay, G., Otzen, D. E., and Fersht, A. R. (1995) *Biochemistry 34*, 1695−1701.
47. Ladurner, G. A., Itzhaki, L. S., de Prat Gay, G., and Fersht, A. R. (1997) *J. Mol. Biol. 273*, 317−329.
48. Sancho, J., and Fersht, A. R. (1992) *J. Mol. Biol. 224*, 741−747.
49. Kippen, A. D., and Fersht, A. R. (1995) *Biochemistry 35*, 1464−1468.
50. Kippen, A. D., Sancho, J., and Fersht, A. R. (1994) *Biochemistry 33*, 3778−3786.
51. Robinson, C. R., and Sauer, R. T. (1996) *Biochemistry 35*, 13878−13884.
52. Predki, P., and Regan, L. (1995) *Biochemistry 34*, 9834−9839.

BI990498L